Computational prediction and experimental analysis of the nanoparticle-protein corona

Hasenkopf, Ingrid; Mills-Goodlet, Robert; Johnson, Litty; Rouse, Ian; Geppert, Mark; Duschl, Albert; Maier, Dieter; Lobaskin, Vladimir; Lynch, Iseult; Himly, Martin

DOI:
10.1016/j.nantod.2022.101561

Nano Today 46 (2022) 101561

Contents lists available at ScienceDirect

Nano Today

journal homepage: www.elsevier.com/locate/nanotoday

Computational prediction and experimental analysis of the nanoparticle-protein corona: Showcasing an *in vitro-in silico* workflow providing FAIR data

Ingrid Hasenkopf[a], Robert Mills-Goodlet[a], Litty Johnson[a], Ian Rouse[b], Mark Geppert[a], Albert Duschl[a], Dieter Maier[c], Vladimir Lobaskin[b], Iseult Lynch[d], Martin Himly[a,*,1,2]

[a] *Div. Allergy & Immunology, Dept. Biosciences & Medical Biology, Paris Lodron University of Salzburg, Austria*
[b] *School of Physics, University College Dublin, Belfield Dublin 4, Ireland*
[c] *Biomax Informatics AG, Planegg, Germany*
[d] *School of Geography, Earth and Environmental Sciences, University of Birmingham, Edgbaston, B15 2TT Birmingham, United Kingdom*

ARTICLE INFO

Article history:
Received 3 March 2022
Received in revised form 29 June 2022
Accepted 17 July 2022
Available online 23 July 2022

Keywords:
Nanoparticle
Protein corona
Multiscale modelling
Metadata completeness

ABSTRACT

Extensive investigation and characterisation of nanoparticle-protein conjugates are imperative to assess potential nanoparticle-induced hazards for humans and the environment, predict adverse biological effects, and identify suitable nanoparticles for medical applications. Investigating the formation of the nanoparticle protein corona solely based on experimental analysis is currently very time-consuming and cost-intensive. Therefore, development of prediction tools based on *in silico* modelling is much-needed in order to provide viable alternative approaches and accelerate nanomaterial risk assessment at the early development stage. This work aimed to validate currently emerging *in silico* protein corona modelling tools with experimental results and to reveal the models' potentials and limitations thereby contributing to the improvement of their predictive power. Comprehensive data and metadata sets of the obtained *in vitro* and *in silico* results were collected and annotated in the NanoCommons Knowledge Base to facilitate data Findability, Accessibility, Interoperability, and Reusability (FAIRness) in nanosafety assessment. *In silico* protein corona predictions (*in silico* modelling with UnitedAtom) and *in vitro* investigation of corona formation (binding and selectivity studies with eight different proteins, mixtures thereof, and an allergenic effector cell degranulation assay) on differently coated SiO_2 nanoparticles were aligned and the results, in the first run, revealed substantial deviations. Therefore, we attempted to identify the potential and limitations in the modelling and provided recommendations to improve the model. Similar iterative approaches, as described here, based on the verification *versus* rebuttal of data from *in silico* procedures by *in vitro* analyses, complemented by comprehensive data and metadata collection according to the FAIR principles, are expected to help optimise future prediction certainties and improve *in silico* modelling.

Introduction

Engineered nanoparticles (NPs) have gained great interest in biomedical sciences over the past decades due to their ability to directly interact with the intra- and extracellular machinery. Since biological molecules are in the same size range as NPs, interference with cellular processes is possible [1,2]. This led to highly active research on bio-nano interactions and the development of nanomaterials for biomedical applications, ranging from drug delivery and vaccines to molecular imaging and bio-detection [3,4]. Silica (SiO_2) NPs are among the most widely produced nanomaterials globally, with various applications in the construction industry, but also in cosmetics, dentistry, medicine, and automotive tyre production [5,6]. This widespread use leads to an elevated chance of exposure to SiO_2 NPs in occupational settings and for consumers, as well as of release of SiO_2 NPs into the environment. Therefore, understanding of bio-nano interactions is essential for the comprehensive assessment of potential human and environmental hazards and the avoidance of adverse effects when exploiting NPs for biomedical applications [7].

* Correspondence to: Div. Allergy & Immunology, Dept. Biosciences & Medical Biology, Hellbrunnerstrasse 34, 5020 Salzburg, Austria.
E-mail address: martin.himly@plus.ac.at (M. Himly).
[1] www.plus.ac.at/himly
[2] http://orcid.org/0000-0001-5416-085X

https://doi.org/10.1016/j.nantod.2022.101561

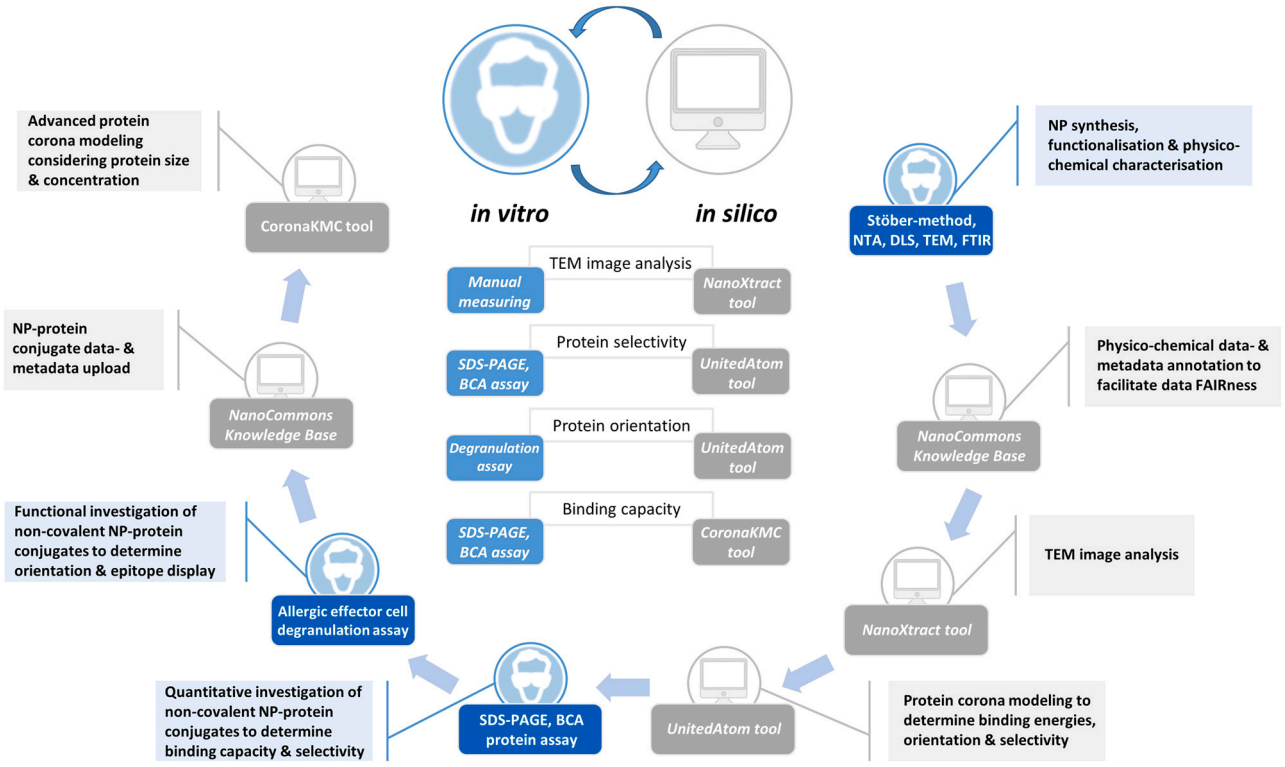

Fig. 1. Overview of experimental-computational workflow performed during this study. Applied *in vitro* assays with annotated data shown in blue, deployed in silico tools with annotated data in grey. Alignments of *in vitro* assays with in silico tools for the respective research questions depicted in the center.

When NPs come in contact with proteins, *e.g.*, after entering a biological fluid, proteins besides diverse other (bio)molecules, immediately associate with them, based on abundance and affinity, coat the NP surface to form the so-called protein corona, or in "real-life" a highly complex (bio)molecular corona. Possible conformational alterations, specific orientations or changes in epitope accessibility (hiding/masking, accumulation, exposure of novel epitopes) of the adsorbed proteins may trigger adverse biological effects. Thus, the protein corona controls the biological identity of the NP and becomes a determinant for the biological activity of the NP [8]. Consequently, extensive investigation of protein corona formation is imperative to assess the effects of surface adsorption of biomolecules onto NPs on immune safety and biocompatibility [9], an aspect of particular relevance in the field of nanomedicine.

Investigating the protein corona of NPs, exclusively based on experimental analysis in the lab, is time-consuming and cost-intensive. Additionally, ethical considerations regarding animal testing should not be neglected [10]. Therefore, *in silico* modelling approaches to predict NP-protein interactions and the resulting biological outcomes offer enormous potential to complement and accelerate nano-related risk assessment while circumventing the drawbacks of experimental analysis. To develop data-driven computational modelling tools with high predictive power, nanomaterial libraries with comprehensive, high-quality data- and metadata sets are required. These should contain a broad range of physicochemical NP characterisation parameters, such as primary particle size, shape, hydrodynamic diameter, chemical composition, surface coating and charge, as well as data on environmental and bio-nano interactions and resulting biological effects [11]. Various challenges in generating these high-quality datasets have been recognized, such as the relatively high heterogeneity of characterisation data in the literature, unsatisfactory completeness and availability levels [12]. Therefore, initiatives for suitable nanomaterial data curation were promoted over the past decade. These comprise workflow descriptions, evaluation criteria for different modelling needs and examples of experimentally generated or literature-based datasets suitable for modelling approaches [13,14].

Here, we aimed to validate currently available *in silico* protein corona modelling tools *vs.* experimental results and to identify their potentials and limitations. Such analysis may help to improve the prediction capabilities of the bio-nano interaction tools. To ensure data FAIRness (findable, accessible, interoperable and reusable), the comprehensive experimental and computational data- and metadata-sets generated from the study were fully annotated with nanosafety ontology terms and aligned with recently defined workflows for metadata capture to ensure FAIR nanosafety data [15,16]. All *in vitro* and *in silico* results and the associated metadata are available *via* the NanoCommons Knowledge Base (NC KB) (https://ssl.biomax.de/nanocommons/), which provides an experiment-to-informatics *in vitro-in silico* workflow for the generation of (FAIR) data [17] for nanosafety assessment.

The formation of the NP protein corona is governed by both specific and non-specific molecular interactions. The non-covalent interactions between NPs and proteins strongly depend on several physicochemical characteristics of the NPs, the proteins and the surrounding environment. NP shape, size, surface charge and hydrophobicity were shown to be key parameters influencing the interactions [18–20]. It is widely recognized that the composition of the protein corona varies for different types of NPs, but the specific characteristics determining this variance have not been clearly identified so far [21]. Therefore, directly relating specific characteristics of NPs to adsorption affinities of proteins could form the basis of predictive *in silico* tools as part of Safe-by-Design schemes, or *in silico* models for material optimisation at the product development stage. We used the recently developed multi-scale modelling tool UnitedAtom, which is integrated into the NC KB to predict the corona composition for selected NPs. This tool directly relates characteristics of NPs to protein binding affinities, which allows ranking of the

proteins by their adsorption affinities thus providing an insight into the composition of the acquired protein corona [22]. The output of this tool can be used for more advanced corona modelling using a recently developed hard-sphere model (CoronaKMC) [23] to account for competition between proteins and the effects of protein concentration and size. Fig. 1 overviews the experimental-computational workflow pursued in this study depicting all assays performed and tools deployed as well as the respective alignments between *in vitro* and *in silico* data.

The main objectives of our *in silico* and *in vitro* analyses were (i) to quantify (computationally and experimentally) the selective binding of proteins onto the surface of differently coated SiO_2 NPs, (ii) to elucidate (computationally) the preferred orientations of the adsorbed proteins, and (iii) to investigate (computationally) whether structural changes, resulting in (experimentally determined) altered biological effects or functions of the protein, could be induced upon protein binding to NPs. For this purpose, SiO_2 NPs were synthesised and functionalised with three different surface coatings (amino-, carboxyl-, or isopropyl-groups) to determine the possible impact of varying physicochemical properties, such as surface charge and hydrophobicity, on protein corona formation. Eight different model proteins, mainly allergens as they provide a genuine assay for experimentally addressing epitope accumulation/masking, were applied for corona studies to determine the binding capacity of the differently coated NPs and to reveal a possible selectivity in binding due to different adsorption affinities of the allergens. The major birch pollen allergen Bet v 1 was employed for use in an allergenic effector cell degranulation assay to investigate the potentially preferred binding orientations or conformational changes leading to altered biological effects of the allergen, namely changes in the allergenic response upon NP adsorption. This enables a direct assessment of potential risks and biological responses of the respective allergen-NP conjugates as well as further refinement of the corona prediction model. We critically assessed the validity and accuracy of the predictions of the *in silico* model against the experimental data and developed recommendations for improvement of the model. The well-characerized but simplified model applied here was based on eight proteins, and mixtures thereof, interacting with bare silica NPs and three particle surface modifications. This reductionist approach was chosen intentionally to circumvent the secondary (cooperative) effects from further interactions between bound proteins and other (bio)molecules, such as lipids or metabolites. This simplification is essential in order to achieve a quantitative picture of protein corona formation kinetics that is not obscured by random or irrelevant (for our purposes) factors of highly complex "real-life" scenarios that are beyond the capacity of currently emerging corona prediction models. This 8-protein mixture should, however, allow evaluation of the utility of biomolecule binding affinities as a predictor of corona composition and enable co-development and systematic improvement to the model's predictive capability, such that greater trust in predictions based on whole proteomes (*e.g.,* full serum) may be established in the near future.

Materials and methods

Nanoparticle synthesis and functionalisation

SiO_2 NPs were synthesised *via* an ammonia-catalysed reaction of tetraethylorthosilicate (TEOS) with ethanol and water as previously described [24]. A mixture of 200 mL ethanol absolute (Carl Roth, Karlsruhe, Germany) and 36 mL pure water was heated to the required reaction temperature of 75 °C in a water bath. Then, 10 mL aqueous ammonia 25 wt% (Merck KGaA, Darmstadt, Germany) was added and after an equilibration time of 10–15 min 15 mL TEOS (Sigma-Aldrich, St. Louis, MO, USA) was added quickly. After 2 h reaction time under intense stirring (500 rpm), the resulting SiO_2 dispersion was separated by 1-hour centrifugation at 6000 *g* and washed three times with pure water. The particles were then suspended in ethanol and dried at 80 °C for 12 h in a beaker in a dry cabinet (referred to hereafter as the bare SiO_2 NPs).

Modification of the bare SiO_2 NPs with NH_2 groups was conducted as previously described [25] with minor adaptations. 200 mg 3-aminopropyltriethoxysilane (APTES, Sigma-Aldrich, St. Louis, MO, USA) was dissolved in 20 mL deionized water and kept at room temperature (RT) for 2 h under magnetic stirring during which a hydrolysis reaction occurred. A fine dispersion of 1 g SiO_2 NPs dissolved in 25 mL ethanol was added to the reaction mixture and kept at 70 °C for 24 h under magnetic stirring. The functionalised SiO_2 NPs were dried at 80 °C for 24 h.

For modification of the bare SiO_2 NPs with COOH groups, 500 mL water was warmed up to 80 °C in a water bath under magnetic stirring (250–300 rpm). 1.5 mL 11-(triethoxysilyl)undecanoic acid (TSUA, synthesised in house, described elsewhere [26]) and 15 mg SiO_2 NPs were added and the mixture was left to react for 2 h. Afterwards, the water amount was reduced to approx. 200 mL by rotary evaporation followed by dialysis for three days (MWCO: 10–20 kDa). The particle dispersion was then concentrated to 40 mL by removing more water *via* rotary evaporation, followed by 1 min centrifugation at 1700 *g* to remove bigger particle aggregates.

Functionalisation of the bare SiO_2 NPs with C_3H_7 groups was conducted likewise the TSUA-coating, using propyltrimethoxysilane (PTMO, abcr GmbH, Karlsruhe, Germany) instead of TSUA.

For dispersion of the bare and APTES-coated NPs, 10 mg of particles were suspended in 10 mL H_2O and ultrasonicated in an Elmasonic S 100 sonication bath (Elma, Singen, Germany) for 30 min

Nanoparticle characterisation

The primary particle size of the four differently coated SiO_2 NPs was determined by transmission electron microscopy (TEM). 2 µL NP dispersion (1 mg mL^{-1}) were dried overnight on a lacey carbon-coated copper TEM grid and the measurement was performed on a JEM F200 (JEOL, Freising, Germany) electron microscope in TEM mode operated at 200 kV. Primary particle size was determined by calculating the mean ± SD of min. 25 particles *via* image processing with ImageJ [27] and manual measuring. Additional image analysis was performed with the nanomaterials image analysis tool NanoXtract [28] which is accessible directly from the NP entry in the NC KB (https://ssl.biomax.de/nanocommons/bioxm_portal/bin/view/BioXM/NanoXtract).

To determine the hydrodynamic radius of the SiO_2 NPs in suspension, nanoparticle tracking analysis (NTA) and dynamic light scattering (DLS) was performed. For NTA measurements, the NPs were diluted in MilliQ water to a final concentration of 0.1 µg mL^{-1} and observed using the NanoSight LM 10 instrument (Malvern, Malvern, UK). Measurements were performed with a red 638 nm laser and the standard measurement protocol with 10 captures per measurement and 20 s capture duration. The ZetaSizer Nano ZS (Malvern, Herrenberg, Germany) was used to determine the hydrodynamic radius *via* DLS and the ζ-potential of the differently coated SiO_2 NPs *via* electrophoretic light scattering (ELS). The NPs were diluted in MilliQ water or citrate buffer (10 mM, pH 4) to a final concentration of 10 µg mL^{-1} and measured in a clear disposable zeta cell (Malvern, DTS1070).

To investigate the presence of different functional groups on the SiO_2 NPs´ surface with Fourier transform-infrared spectroscopy (FTIR), 50 µg NP dispersions were dried overnight at 80 °C in a beaker in a dry cabinet. FTIR spectra were obtained using a Bruker Tensor 27 FTIR spectrometer (Bruker Optics, Ettlingen, Germany) equipped with an ATR (MIRacle ATR, Pike technologies, Fitchburg, WI, USA) accessory and the Opus Software (Bruker Optics Version 6.5).

Nanoparticle-protein conjugate formation

Proteins were coupled to NPs as previously described [29] in either 10% or 20% protein-NP ratio (w/w) in 500 µL citrate buffer (10 mM, pH 4), sodium phosphate buffer (10 mM, pH 7.4), Tris buffer (10 mM, pH 9) or dH_2O for 16 h on a rotational wheel at 4 °C. For couplings, the proteins Lysozyme (from hen egg white, lyophilized powder, Sigma-Aldrich), Ovalbumin (from hen egg white, lyophilized powder, Sigma-Aldrich), Beta-lactoglobulin a (from bovine milk, lyophilized powder, Sigma-Aldrich), Serotransferrin (apotransferrin human powder, Sigma-Aldrich), birch pollen extract (Betula pendula, ThermoFisher Scientific) and the recombinant major birch pollen allergen Bet v 1, produced as described by Grotz et al. [29], were used. To prepare the birch pollen extract (BPE) for couplings, 100 mg were suspended in 1 mL distilled water (dH_2O) for 1 h on a sample shaker (700 rpm). Afterwards, the dispersion was centrifuged (10 min, 16,000 *g*) and the collected supernatant was diluted 1:2 with MilliQ water for incubation with the NPs.

Protein quantification

After the incubation, samples were centrifuged twice for 1 h at 16,000 *g* and 4 °C to avoid contamination of the supernatant with parts of the NP-protein pellet. The pellet was suspended in dH_2O and the protein content of the pellet and supernatants was determined using the BCA (bicinchoninic acid) protein assay and sodium dodecyl sulfate polyacrylamide gel electrophoresis (SDS-PAGE) with subsequent densitometric analysis. The BCA assay was performed according to the microplate procedure protocol provided by the manufacturer (Pierce™ BCA Protein Assay Kit User Guide, ThermoFisher Scientific). For SDS-PAGE, the protein samples were diluted in 4x reducing buffer (250 mM Tris, 8% SDS, 40% glycerol, 10% ß-mercaptoethanol, 0.04% Bromphenol blue) and heated at 95 °C for 10 min for heat denaturation of the proteins. Samples were loaded on a 15% polyacrylamide gel together with a molecular weight marker (Pierce™ Unstained Protein MW Marker, Thermo Scientific™) and control samples with known protein concentration for quantitative comparison. The gels were stained with Coomassie R250 Staining solution (0.1% Coomassie Brilliant Blue R250, 50% methanol, 10% acetic acid) and imaged with the ChemiDoc Imaging system (ChemiDoc MP, Bio-Rad). The protein contents were quantified using the ImageLab™ (Version 6.0.1 build 34, Bio-Rad) quantification tool by calculating the relative quantity of protein in the samples compared to the protein quantity in the control sample. Representative pdf reports and (meta)data for all evaluations (3 repeats each) are available at https://doi.org/10.5281/zenodo.4609839.

Allergic effector cell degranulation assay

To investigate alterations in the allergic response to Bet v 1 upon adsorption onto the four differently coated SiO_2 NPs, a mediator release assay was performed as previously described [30] with minor adaptations. Rat basophilic leukaemia cells (RBL-2H3) transfected with the human high affinity-IgE receptor (huRBL cells) were cultured in 75 cm^2 tissue culture flasks until 80% confluency at 37 °C in sterile, humidified conditions with 5% CO_2 in MEM (Minimum essential medium Eagle, Sigma Aldrich, Vienna, Austria) supplemented with 4 mM L-glutamine, 5% heat-inactivated fetal calf serum and 0.5 mg mL^{-1} Gentamycin 418 (hereafter referred to as complete MEM (cMEM)). AG8 cells (ATCC, Wesel, Germany) were cultured in Opti-MEM I + Glutamax (reduced serum medium, Gibco™ ThermoFisher Scientific, Paisley, UK) supplemented with 5% heat-inactivated fetal calf serum and 1 mg mL^{-1} PenStrep at 37 °C in sterile, humidified conditions with 5% CO_2. The huRBL cells were harvested *via* trypsinisation, resuspended in fresh cMEM at 1×10^6 cells mL^{-1} and aliquoted (100 µL) into 96-well flat-bottomed cell culture plates and incubated overnight at 37 °C, 5% CO_2. The cells were sensitised with blood sera (IgE) from six patients allergic to Bet v 1. Patient sera were provided by the Allergy Clinic Salzburg (RAST classes ≥ 3). The procedure was approved by the local Ethics Committee of the Allergy Clinic Salzburg (No. 415-E/1398/4–2011). Sera were pre-incubated for 1 h at 37 °C and 5% CO_2 with AG8 cells for complement system depletion. After centrifugation (250 *g*, 5 min), the supernatants of the sera were aliquoted (100 µL) into the respective sample wells of the 96-well huRBL cell plates followed by overnight serum incubation at 37 °C and 5% CO_2, and then washed three times with cMEM. Afterwards, 100 µL of various concentrations of different SiO_2 NP-Bet v 1 conjugates and Bet v 1 only (1000 ng mL^{-1} to 0.0001 ng mL^{-1}) were added to the huRBL cells and incubated for 1 h at 37 °C and 5% CO_2. To determine the total β-hexosaminidase content of the cells, 10 µL of 10% Triton X-100 was added to separate aliquots of the cells (in quintuplicates). 50 µL supernatant of the antigen-incubated and positive and negative control cells was added to the fluorogenic substrate 4-methyl umbelliferyl-N-acetyl-β-D-glucosaminide (Sigma-Aldrich, St. Louis, MO, USA) and incubated for 1 h at 37 °C and 5% CO_2. The reaction was stopped by adding 100 µL glycine buffer (pH 10.7, 0.2 M) and the fluorescence intensity was measured at an excitation wavelength of 360 nm and an emission wavelength of 465 nm using 25 flashes using a microplate reader (Tecan M200pro). The specific release (%) of the huRBL cells induced by different NP-Bet v 1 conjugates was calculated using the following equation:

$$\%\text{release} = \frac{\text{fluorescence of sample} - \text{fluorescence of blank}}{\text{fluorescence of 100\% release (positive control)} - \text{fluorescence of blank}} \times 100\%$$

The specific release in percentage was then used to determine the antigen concentration for half-maximum mediator release (ng mL^{-1}) expressed in a scatter plot with a logarithmic scale.

Cell viability was determined using the MTT assay as previously described [31].

In silico protein corona modelling

In silico protein corona predictions of the four differently coated SiO_2 NPs interacting with the same proteins as used in the experimental assay (Section 2.3) and listed in Table 1 were accomplished with the modelling tool UnitedAtom [22], available through the NC KB (https://ssl.biomax.de/nanocommons/bioxm_portal/bin/view/BioXM/CoronaOverview). This tool uses physics-based atomistic simulations to model bio-nano interactions and calculates adsorption energies and preferred orientations of the proteins on the NP surface. This allows ranking of the different proteins according to their adsorption affinities for specific NPs, and to predict the kinetics of the protein corona formation. To model the desired NP-protein interaction, seven parameters of the UnitedAtom configuration file were adjusted. First, the 3D structure of the protein of interest was added by entering the respective PDB-ID (https://www.rcsb.org/) as

Table 1
Properties and identifications of proteins used for experimental analysis and for in silico modelling. Theoretical pI (isoelectric point) value and MW (Molecular Weight) determined by Expasy ProtParam (https://web.expasy.org/protparam/).

Protein	UniProt ID	IUIS	PDB	pI	MW
Bet v 1	P15494	Bet v 1.0101	4A88	5.39	17.4 kDa
Bet v 2	P25816	Bet v 2.0101	1CQA	5.02	14.1 kDa
Bet v 4	Q39419	Bet v 4.0101	1H4B	4.76	9.4 kDa
Bet v 6	Q9FUW6	Bet v 6.0102	–	6.73	34.2 kDa
Beta-lactoglobulin a	P02754	Bos d 5.0101	1CJ5	4.83	18.3 kDa
Ovalbumin	P01012	Gal d 2.0101	1UHG	5.19	42.7 kDa
Lysozyme	P00698	Gal d 4.0101	1DPX	9.32	14.3 kDa
Serotransferrin	P02787	–	6JAS	6.70	75.2 kDa

Table 2
Physicochemical properties of bare and differently coated SiO_2 NPs. Size (TEM): primary particle diameter in nm calculated from the mean ± SD of minimum 25 particles. Size (NTA): Average ± SD of the hydrodynamic diameter mode values of three measurements. Size (DLS): Average ± SD of mean values from number-weighted distribution analysis of three measurements. ζ-potentials in mV determined by ELS measurement of NPs resuspended in water (actual pH value of suspensions determined by pH test strips) or in pH 4 citrate buffer, mean ± SD of three measurements.

Property	Bare	APTES	TSUA	PTMO
Size [nm] (TEM)	58.8 ± 4.4	55.1 ± 5.4	58.8 ± 4.3	99.0 ± 14.5
Size [nm] (NTA)	81.8 ± 9.3	104.9 ± 10.8	80.6 ± 7.0	113.9 ± 9.9
Size [nm] (DLS)	89.3 ± 16.9	81.1 ± 3.7	83.8 ± 25.5	97.4 ± 6.2
ζ-pot. [mV] H_2O	-28.8 ± 0.2	26.9 ± 0.6	-31.0 ± 4.0	-23.9 ± 1.4
pH of NPs in H_2O	7	8.5	4.75	7
ζ-pot. [mV] pH 4	-8.5 ± 0.7	0.8 ± 0.6	-23.1 ± 0.7	-4.5 ± 0.1

listed in Table 1, or in the case of Bet v 6, where no PDB structure is available, a 3D model was generated with I-TASSER (https://zhanglab.ccmb.med.umich.edu/I-TASSER/) and used for the modelling. Then, the NP radius was entered by using the hydrodynamic radius determined by NTA measurements (Table 2) of the respective SiO_2 NP. Pre-calculated potentials of mean force and Hamaker constants for amorphous silica surfaces with all 20 proteinogenic amino acids (AA) were used. Finally, the electrostatic potential of the desired NP (ζ-potential values listed in Table 2) was entered and the interaction parameters (surface, core, electrostatic) to be incorporated into the calculations were defined. The calculated adsorption energies for all possible orientations (2592 orientations upon rotation in 5° steps of the angles φ and θ) were then used to create a heatmap using a Plotmap tool [22] which displays the adsorption energies of the corresponding angles φ and θ and outputs the lowest energy and the corresponding degrees of rotation.

The predicted binding energies can be directly compared to the observed corona abundances under the assumption that a more strongly binding protein is likely to be more abundant in the corona (even if present at lower abundance in a biofluid). This simple analysis, however, excludes effects arising from the differing biological concentrations for each protein and the area occupied by each protein on the NP, both of which are known to influence the corona formation [23,32,33]. To estimate the steady-state corona composition, we employed a combined kinetic Monte Carlo (KMC) and rate equation approach as described in [23]. In brief, this approach simulates the sequential adsorption and desorption of spherical proteins to a spherical NP using a model in which proteins occupy a given area, A_i, of the surface of the NP based on the projection of the protein onto the NP. Here, a "protein" refers to a given species and orientation or average over orientations as discussed later. Proteins arrive at the surface of the NP at a rate given by $k_{a,i} \quad n_i\,[C_i]$, where $k_{a,i}$ is an adsorption rate constant, n_i is the number of available binding sites given by the surface area of the NP divided by A_i, and $[C_i]$ is the molar concentration of that protein in the bulk. This concentration is calculated from the initial concentration $[C_i(0)]$, the concentration of NPs $[C_{NP}]$ and the average number of bound proteins per NP $\langle N_i \rangle$ (summed over all orientations of that protein) according to $[C_i] = [C_i(t=0)] - \langle N_i \rangle [C_{NP}]$, which models depletion of proteins due to binding to the NP. In the KMC simulations of this process, arriving proteins are assigned a randomly generated position and accepted if their projection on the surface of the NP does not overlap with pre-existing proteins. Adsorbed proteins desorb at a rate given by the desorption rate constant $k_{d,i}$. The KMC algorithm, as implemented in the CoronaKMC tool available as part of the UnitedAtom repository (UnitedAtom code repository https://bitbucket.org/softmattergroup/unitedatom/src/master/), advances from one event (trial adsorption or the desorption of a bound protein) to the next to enable the simulation of extended periods and outputs the number of bound proteins of each type at pre-defined time intervals. The rate equation model is given in [23] and to simplify solving the set of differential equations we do not incorporate the effects of protein depletion, that is, all concentrations in solution remain fixed. For this work, we use spheres of varying radii and binding affinities to represent different orientations of each protein, with the output representing the total number of each type of protein summed over orientations. The effective concentration of a particular orientation of a protein is given by $[C_i] sin\,\theta / \sum_\theta \sin\theta$ to correctly account for the density of states on the sphere. We find the effective radius R_i for a given orientation by projecting the carbon-alpha position of each amino acid (AA) bead onto the surface of the NP, performing a convex hull operation on this set of points to obtain the outline of the protein on the NP, and integrating over this region to obtain the total area A_i. Per-site adsorption and desorption rate constants for a given orientation k_a, k_d are chosen such that:

$$k_a / k_d = K_{Eq} = exp(\Delta G / k_B T)$$

where we approximate ΔG by the orientation-specific adsorption energy, $E(\phi, \theta)$. The value of k_a for that orientation is estimated by using diffusion theory to estimate the total rate of collisions between proteins and a NP, $r_{coll} = 4\pi(D_{NP} + D_i)(R_i + R_{NP})[C_i]N_A$, setting this equal to the rate in the model $r_{coll} = k_a [C_i] n_i$, and solving for k_a. We approximate the diffusion coefficients using Stokes-Einstein theory. N_A is Avogadro's number used to ensure k_a is in molar units. The desorption rate k_d is then obtained from k_a, K_{Eq} to ensure that the steady-state populations of proteins are independent of the exact choice of k_a, *i.e.*, the choice of k_a effectively determines only the units of time. 10 NPs are simulated at once to allow for the estimation of $\langle N_i \rangle$. In practice, this allows only the simulation of a short time due to the large size of the NPs. We, therefore, extend the results to the steady-state by numerically solving the rate equations given in [23]. This requires the grouping of protein orientations by size and binding affinity to the NP to produce a more manageable system of differential equations to solve. For each protein, we generate groups consisting of orientations with calculated radii binned in 1 nm steps and binding affinities binned in steps of $1 k_B T$. Within each group, we calculate the predicted number abundances in the mean-field model [23,32,33] and use these to calculate weighted averages of k_a, E_{ads}, R. From these we obtain $k_d = k_a exp(E_{ads})$ as before. In doing so, the initial set of over 10,000 coupled differential equations reflecting the occupation of each orientation of each protein is reduced to a set of 209 equations, which may be numerically integrated using Mathematica [34]. The KMC simulations do not require this step and treat each protein orientation separately, providing a sum over orientations as output to give the total number of bound proteins of each type.

Statistical analysis

Statistical analyses were accomplished with GraphPad Prism 8. For multiple comparisons one-way ANOVA (Analysis of Variance) followed by Tukey´s *post hoc* test was performed. P-values ≤ 0.05 were considered as statistically significant ($^*p \le 0.05$; $^{**}p \le 0.01$; $^{***}p \le 0.001$; $^{****}p \le 0.0001$).

Results and discussion

Physicochemical characterisation of SiO_2 nanoparticles

Primary particle size determination was conducted, first, by calculating the mean ± SD of at least 25 particles of TEM images manually measured with ImageJ and, second, by analysis of the TEM images with the NanoXtract image analysis tool. Both methods gave similar results (Size [nm] (TEM) in Table 2 and Diameter [nm] in Table 3). Additionally, the determined hydrodynamic diameter values (Size [nm] (NTA) and Size [nm] (DLS) in Table 2) showed that

Table 3
NanoXtract image descriptors and primary particle size of the four differently coated SiO_2 NPs. Size (TEM): primary particle size in nm calculated from the mean ± SD of minimum 25 particles manually measured with ImageJ (as per Table 2). The meaning of each of these image descriptors is described in Varsou et al., 2020 [28].

Descriptor	Bare	APTES	TSUA	PTMO
Size [nm] (TEM)	58.8 ± 4.4	55.1 ± 5.4	58.8 ± 4.3	99.0 ± 14.5
Diameter [nm]	59.79 ± 2.11	55.65 ± 8.26	64.66 ± 5.68	99.05 ± 5.31
Circularity	0.83 ± 0.022	0.83 ± 0.021	0.84 ± 0.024	0.85 ± 0.019
Perimeter [nm]	194.42 ± 7.64	175.76 ± 22.76	205.18 ± 18.95	326.59 ± 18.41
Convexity	0.98 ± 0.002	0.99 ± 0.002	0.99 ± 0.002	0.99 ± 9.359
Extent	0.75 ± 0.018	0.73 ± 0.039	0.73 ± 0.032	0.77 ± 0.006
Area [nm^2]	2477.8 ± 208.4	2031.3 ± 513.9	2814.1 ± 524.6	7209.5 ± 817.8
Circularity #2	0.84 ± 0.023	0.83 ± 0.022	0.85 ± 0.024	0.86 ± 0.02
Convexity #2	0.93 ± 0.008	0.94 ± 0.009	0.95 ± 0.006	0.94 ± 0.009
Eccentricity	0.29 ± 0.057	0.36 ± 0.103	0.31 ± 0.084	0.18 ± 0.025
Main Elongation	0.027 ± 0.013	0.036 ± 0.026	0.037 ± 0.021	0.012 ± 0.008
Min. Ferets Diameter [nm]	55.36 ± 2.42	48.94 ± 6.15	58.17 ± 5.68	95.01 ± 5.52
Max. Ferets Diameter [nm]	59.16 ± 2.07	54.97 ± 8.25	63.97 ± 5.71	98.41 ± 5.35
Major Axis [nm]	57.44 ± 2.27	52.43 ± 7.04	61.21 ± 5.54	96.49 ± 5.44
Minor Axis [nm]	54.84 ± 2.56	48.58 ± 6.13	58.08 ± 5.65	94.88 ± 5.68
Boundary Size [nm]	192.41 ± 7.64	173.85 ± 22.91	203.31 ± 18.88	324.59 ± 18.53
Boxivity	0.78 ± 0.008	0.78 ± 0.023	0.79 ± 0.017	0.78 ± 0.005
Roundness	0.95 ± 0.019	0.93 ± 0.037	0.95 ± 0.029	0.98 ± 0.004
Solidity	0.98 ± 0.009	0.97 ± 0.009	0.96 ± 0.013	0.99 ± 0.004

Note: NanoXtract produces two circularity and convexivity values, calculated by different KNIME nodes.

the four differently coated SiO_2 NPs were in a comparable size range (approximately 50–100 nm), so that no size-related difference in protein corona formation should be expected, and therefore all four NP preparations were qualified for further experiments. The agreement of the manually measured primary particle size with the results from the NanoXtract image analysis demonstrated it as a valuable and trustworthy tool for fast and comprehensive image analysis with large data output. However, during the filtering and thresholding process, numerous particles were excluded from the analysis, based on the settings chosen, leading to a decreased statistical significance compared to the manual measurement. In consequence, the analysis tool considered only 8 particles from the bare SiO_2 NP image (Fig. 2A), 21 from APTES- (Fig. 2B), 13 from TSUA- (Figs. 2C) and 5 from the PTMO-coated NP images (Fig. 2D), where the manual analysis was based on 25, 30, 30 and 50 particles for the respective measurements. The higher number of considered particles greatly enhanced the statistical significance of the manually obtained data. It is, therefore, currently not yet advisable to completely substitute manual image analysis with *in silico* tools unless a sufficient number of images is available to allow statistical robustness. NanoXtract has the capability to upload and analyse multiple images to overcome this issue. However, even based on single images, *in silico* image analysis tools are a useful supplement to enrich the data set with additional nanodescriptors that may be used for toxicity prediction algorithms.

Next, surface charge determinations were performed. The different ζ-potential values of the functionalised SiO_2 NPs (Table 2), compared to the bare NPs, demonstrated that the coating with different functional groups was successful. When comparing the ζ-potentials of all four NPs at different pH values, we noticed significant divergence, which was most likely due to the varying availability of H^+ ions, which has previously been reported to influence the electrostatic interactions of the NPs and, hence, also the formation of the protein corona [35]. To further confirm the presence of the different functionalisations on the SiO_2 NPs, besides ζ-potential measurements, FTIR measurements were conducted. The FTIR spectra (Fig. 2E-H) demonstrated the presence of the respective surface functional groups, NH_2 for APTES-coated NPs, COOH for TSUA-coated NPs, and C_3H_7 for PTMO-coated SiO_2 NPs [36,37].

To facilitate data FAIRness, we supplemented the generated data with comprehensive sets of metadata of our experimental analyses, comprising extensive physicochemical NP characterisation as well as *in vitro* investigations and *in silico* predictions of protein corona formation. This data has been deposited in an open-access data repository (DOI: 10.5281/zenodo.4609840) for long-term storage, in addition to annotation into the NC KB to facilitate interactive re-use of the data for future *in silico* modelling approaches. Our NPs can be found with the respective NP-IDs in the NC KB. The assigned NP-IDs of individual particles are, NP01155 for bare SiO_2 NPs, NP01156 for APTES-coated SiO_2 NPs, NP01157 for TSUA-coated SiO_2 NPs and NP01113 for PTMO-coated SiO_2 NPs.

Binding capacity of differently coated SiO_2 NPs and Bet v 1

To determine the binding capacity of the four differently coated SiO_2 NPs with Bet v 1, non-covalent conjugates were made with 10% or 20% protein to NP ratio (w/w) in different buffers with 10 mM (citrate buffer pH 4, sodium phosphate buffer pH 7.4, Tris buffer pH 9). The binding capacity in weight percent was calculated using the following equation:

$$\text{Binding capacity in wt \%} = \frac{\text{Concentration of bound protein} \times 100}{\text{Applied NP concentration}}$$

The highest binding capacity was observed in pH 4 citrate buffer, followed by binding in pH 7.4 and pH 9 buffers for all four SiO_2 NPs (Fig. 3). This is in agreement with previous findings, showing that the optimum pH for the coupling buffer is defined by the pI value of the respective protein and that the binding is most efficient at a pH value slightly below the pI value of the protein [38]. The pI value of Bet v 1 is 5.39 (Table 1, theoretical pI values determined by Expasy ProtParam) [39], which explains the most efficient binding to all SiO_2 NPs in pH 4 buffer, in which the protein is slightly positively charged. The highest binding capacity was observed on TSUA-coated SiO_2 NPs. These NPs possess the most negatively charged surface potential of all four investigated NPs (Table 2) in addition to a highly hydrophobic character due to the long carbon chain provided by TSUA used for the functionalisation. This indicates that electrostatic as well as hydrophobic interactions are crucial for the formation of the protein corona, which coincides with findings from previous studies [8,18].

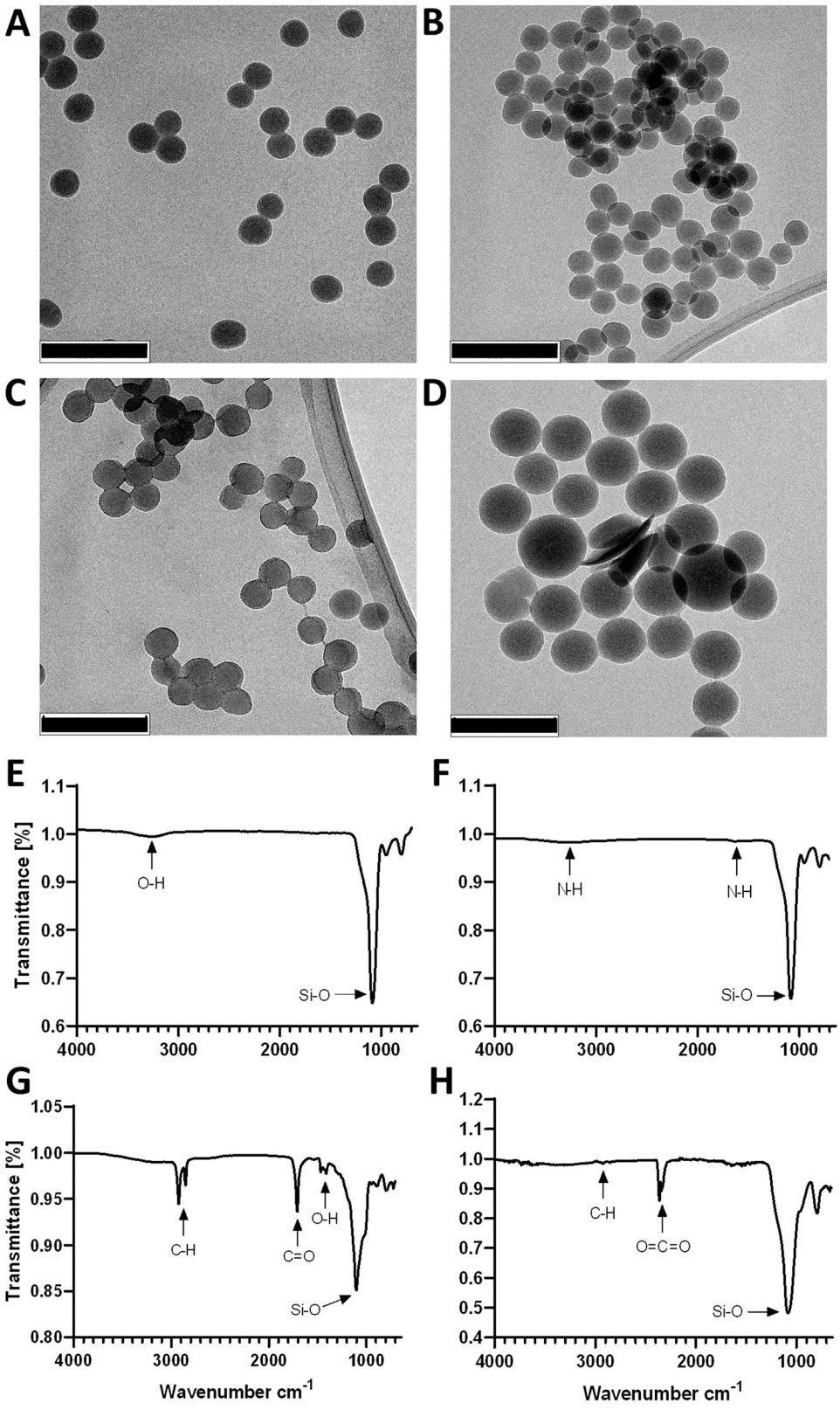

Fig. 2. Characterisation of SiO_2 NPs. (A-D) TEM images of differently coated SiO_2 NPs for determination of primary particle size. (A) bare (B) APTES- (C) TSUA- (D) PTMO-coated SiO_2 NPs, Scale bar: 200 nm. (E-H) FTIR spectra of differently coated SiO_2 NPs, (E) bare (F) APTES- (G) TSUA- (H) PTMO-coated SiO_2 NPs, Transmittance (%) of the samples plotted against Wavenumber cm^{-1}.

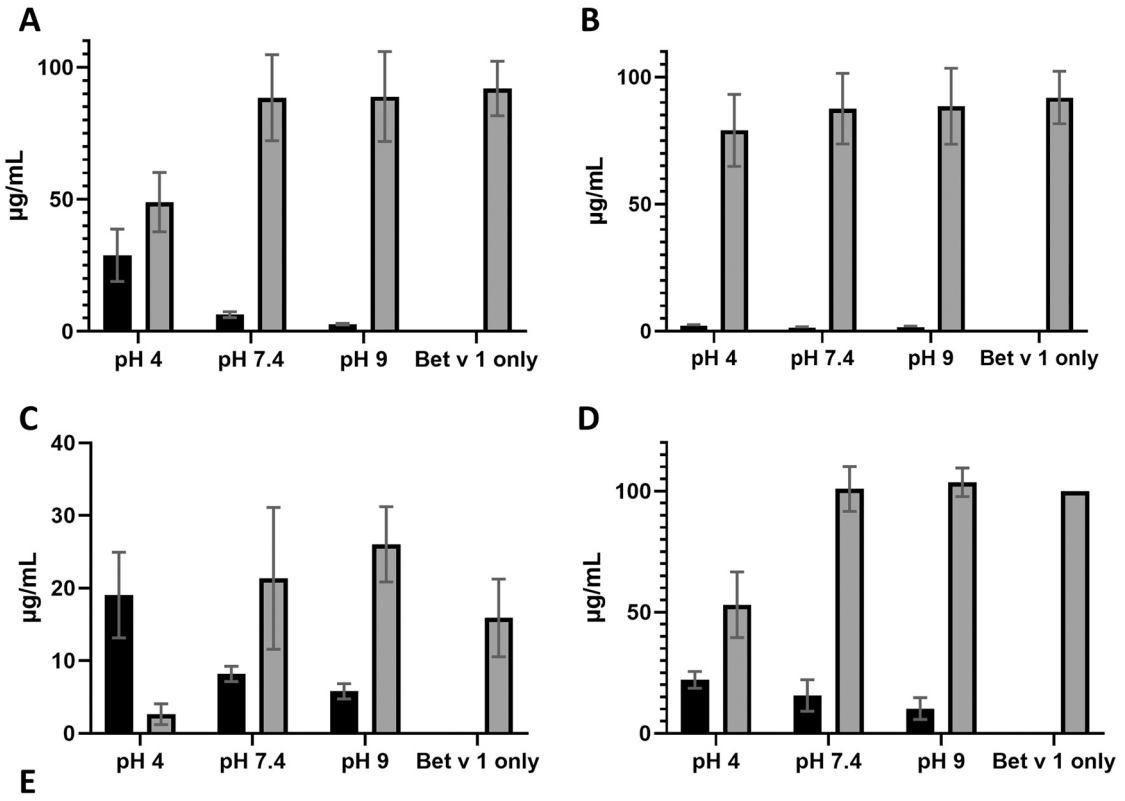

E

	Bare	APTES	TSUA	PTMO
pH 4 buffer	5.8 ± 1.6%	0.4 ± 0.1%	9.5 ± 2.4%	4.4 ± 0.6%
pH 7.4 buffer	1.3 ± 1.8%	0.3 ± 0.1%	4.1 ± 0.4%	3.1 ± 1.1%
pH 9 buffer	0.6 ± 0.1%	0.3 ± 0.1%	2.9 ± 0.4%	2.1 ± 0.7%

Fig. 3. Binding of Bet v 1 on four differently coated SiO_2 NPs. (A) bare (B) APTES- (C) TSUA- (D) PTMO-coated SiO_2 NPs. Black bars: bound protein, Grey bars: unbound protein. Determined in pH 4 citrate buffer, 10 mM; pH 7.4 sodium phosphate buffer, 10 mM; pH 9 Tris buffer, 10 mM. Results of BCA protein assay expressed as µg mL^{-1} of protein in pellet (bound) or supernatant (unbound). Applied protein-NP ratio for conjugate formation: 20% (bare, APTES, PTMO) and 10% (TSUA). Bet v 1 only as control; Graphs show mean ± SD of three experimental repeats. (E) Binding capacity in weight percent of four different SiO_2 NPs with Bet v 1. Mean ± SD of three experimental repeats.

Selective protein binding to SiO_2 NPs – the composition of the protein corona

Protein-NP conjugates with birch pollen extract (BPE) and an artificial protein mix (beta-lactoglobulin a, ovalbumin, lysozyme, serotransferrin) with a 20% protein to NP ratio (w/w) were prepared in pH 4 citrate buffer and in water to investigate potential selective binding. Furthermore, the proteins were ranked according to their binding affinities, to determine the composition of the protein corona. The bare and APTES-coated NPs were used for these investigations due to their diverging surface potentials (Table 2). The results revealed clear differences in the binding behaviour of the different proteins to the two NPs in the different coupling environments (Fig. 4A, B). In water, both ovalbumin (Ova) and beta-lactoglobulin a (BLG) revealed a selectivity for the APTES-coated NPs, while bare SiO_2 NPs showed the highest binding capacity for lysozyme (Lyso). Contrastingly, serotransferrin (Sero) showed preferential binding to the bare SiO_2 NPs at pH 4. This preferential binding to the more negatively charged bare SiO_2 NPs might be explained by Sero's overall positive surface charge at pH 4, according to its pI value (6.7, Table 1). In water, lysozyme (pI 9.3) is positively charged, which promotes binding to the more negatively charged bare NPs, whereas Ova and BLG exhibit a negative surface potential and therefore preferentially bind to the positively charged APTES-coated SiO_2 NPs.

For quantitative comparisons of the proteins present in the BPE, the five most prominent bands of the gel (Fig. 4B) were chosen. Assigning the bands according to their molecular weight to birch pollen allergens, we assumed that band 1 corresponds to Bet v 6 (MW 34.2 kDa), band 4 to Bet v 1 (MW 17.4 kDa) and band 5 to Bet v 2 (MW 14.1 kDa). All five proteins revealed higher binding to the NPs at pH 4 than in water. Considering the pI values of the birch pollen allergens, which all range from 4.7 to 6.7 (Table 1), the results indicate that they promote adsorption onto NPs at a pH value slightly below their pI value, where they exhibit a positive surface potential coinciding with our previous findings described above. Table 4 ranks the proteins according to their binding affinities to the differently coated NPs in pH 4 buffer and water, and thus depicts the composition of the protein corona according to our *in vitro* results. The protein ranked on top represents the most abundant one in the experimentally determined protein corona of the respective NP. The results of the subsequent *in silico* protein corona modelling with UnitedAtom were compared to these results to assess the reliability of the UnitedAtom approach (Table 5).

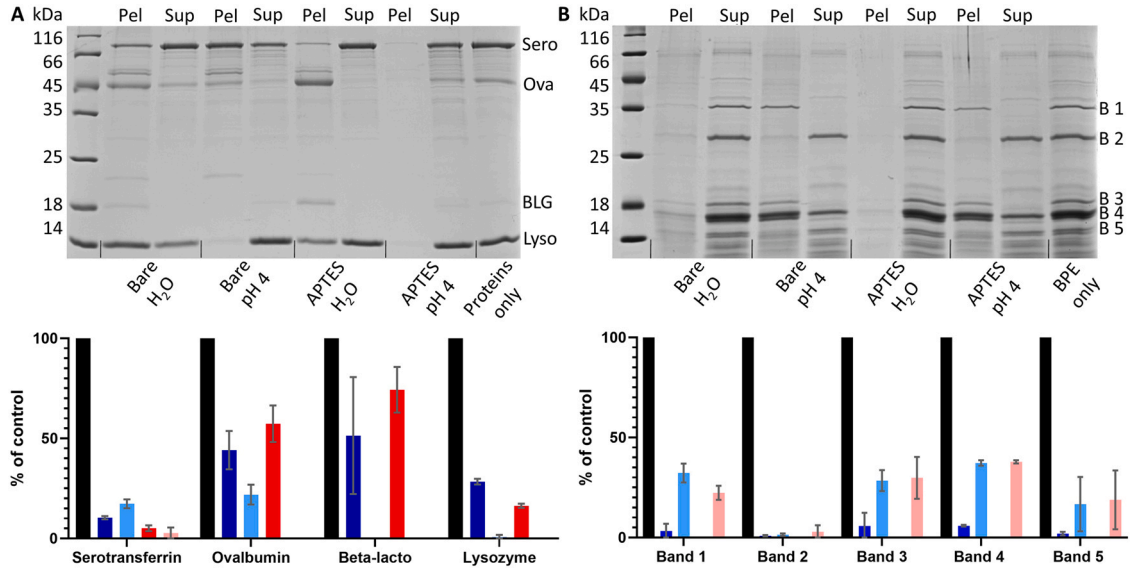

Fig. 4. Selective binding of artificial protein mix and birch pollen extract (BPE) proteins to bare and APTES-coated SiO_2 NPs. (A) SDS-PAGE results of artificial protein mix-NP conjugates, Mix of proteins only as control. (B) SDS-PAGE results of BPE-NP conjugates, BPE only as control, five most prominent bands were chosen for quantitative comparison. Results in histograms expressed as % of control bound to NP, graphs show mean ± SD of three experimental repeats, black bars: control, dark blue bars: Bare SiO_2 in H_2O, light blue bars: Bare SiO_2 in pH 4 buffer, dark red bars: APTES-coated SiO_2 in H_2O, light red bars: APTES-coated SiO_2 in pH 4 buffer, BPE (birch pollen extract), Pel (bound protein in pellet), Sup (unbound protein in supernatant), Sero (Serotransferrin), Ova (Ovalbumin), BLG (Beta-lactoglobulin a), Lyso (Lysozyme), B1-B5 (Band 1-Band 5).

Table 4
Ranking of birch pollen extract (BPE) and artificial protein mix according to binding capacity on bare and APTES-coated SiO_2 NPs determined *in vitro* in H_2O or pH 4 buffer. Five most prominent bands of BPE gel were chosen for quantitative comparison and according to their molecular weight assigned to the main birch pollen allergens. Protein bound to NPs as % of control in brackets. Sero (Serotransferrin), Ova (Ovalbumin), BLG (Beta-lactoglobulin a), Lyso (Lysozyme).

Bare	Bare	APTES	APTES
H_2O	pH 4	H_2O	pH 4
Band 4 (Bet v 1, 37.3%)	Band 4 (Bet v 1, 37.8%)	–	Band 4 (Bet v 1, 5.9%)
Band 1 (Bet v 6, 32.3%)	Band 3 (29.8%)	–	Band 3 (5.7%)
Band 3 (28.5%)	Band 1 (Bet v 6, 22.4%)	–	Band 1 (Bet v 6, 3.3%)
Band 5 (Bet v 2, 16.7%)	Band 5 (Bet v 2, 18.8%)	–	Band 5 (Bet v 2, 1.9%)
Band 2 (2.9%)	Band 2 (1.4%)	–	Band 2 (0.9%)
BLG (51.4%)	Ova (21.9%)	BLG (74.3%)	Sero (2.7%)
Ova (44.1%)	Sero (17.4%)	Ova (57.3%)	–
Lyso (28.4%)	Lyso (0.77%)	Lyso (16.3%)	–
Sero (10.3%)	BLG (0%)	Sero (5.1%)	–

Decreased allergic response towards Bet v 1-TSUA-coated SiO_2 NP conjugates

To investigate possible structural changes or specific orientations of Bet v 1 upon adsorption onto the four differently coated SiO_2 NPs, which would lead to destruction or inaccessibility of IgE epitopes, alterations in the allergic response were investigated using the huRBL mediator release assay. The results in Fig. 5 indicated that, in general, a higher concentration of Bet v 1 was needed to achieve half-maximal mediator release when it was bound to all four SiO_2 NPs compared to when free in solution. However, statistically significant results were obtained only when Bet v 1 was bound to TSUA-coated SiO_2 NPs. We thus concluded that a significantly decreased release of the mediator β-hexosaminidase occurred when Bet v 1 was adsorbed onto these NPs. This generation of a less allergenic form of Bet v 1, when it was bound to TSUA-coated NPs, indicates a change in the structure or a specific orientation of Bet v 1 leading to altered IgE epitope accessibility (at least for the patients used). The circumstance that particle association can have an effect on the immune response, has previously been shown for Bet v 1 bound to SiO_2 NPs [40].

Table 5
Minimum adsorption energies (E_{ad}) for proteins of interest on four different SiO_2 NPs determined in silico with UnitedAtom. All values are reported in units of k_BT (Boltzmann constant at Temperature in Kelvin), T = 300 K. 1 k_BT = 2.494 kJ/mol. ζ-potentials of particles used for modelling were determined in H_2O and pH 4 buffer. Proteins are ranked by descending adsorption energy on bare SiO_2 NPs, grouped as artificial protein mix and BPE proteins.

Protein	E_{ad}/k_BT Bare ζH_2O / pH 4	E_{ad}/k_BT APTES ζH_2O / pH 4	E_{ad}/k_BT TSUA ζH_2O / pH 4	E_{ad}/k_BT PTMO ζH_2O / pH 4
Ovalbumin	-48.73 / -49.36	-51.66 / -48.96	-48.36 / -48.59	-49.59 / -50.14
Serotransferrin	-39.21 / -37.51	-35.02 / -37.04	-39.91 / -39.16	-39.61 / -37.65
Lysozyme	-33.99 / -32.59	-29.71 / -31.99	-34.02 / -33.57	-34.02 / -32.63
Beta-lactoglobulin a	-31.25 / -32.92	-35.62 / -33.53	-30.89 / -31.77	-31.13 / -33.22
Bet v 6	-36.38 / -34.64	-33.09 / -34.58	-35.86 / -36.82	-35.78 / -33.52
Bet v 2	-30.24 / -31.36	-33.26 / -31.22	-29.61 / -30.13	-30.79 / -31.85
Bet v 1	-29.05 / -30.21	-31.81 / -30.2	-29.51 / -29.35	-29.48 / -31.01
Bet v 4	-22.42 / -23.28	-24.01 / -23.29	-22.33 / -22.11	-22.25 / -23.36

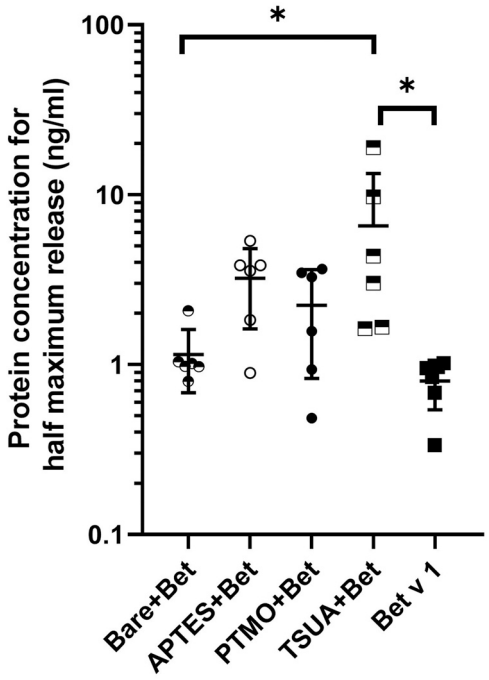

Fig. 5. Basophil mediator release of allergic patient sera upon incubation with Bet v 1 only or allergen-NP conjugates. Protein concentration for half maximum release in ng mL^{-1} presented on a log scale. Scatter plot shows mean ± SD of 6 different patient sera. Statistical analysis with GraphPad Prism 8; Ordinary one-way ANOVA followed by Tukey´s *post hoc* test for multiple comparisons; $^{*}p \leq 0.05$.

The investigation of potential structural alterations of proteins upon adsorption onto NPs is crucial to predict possible adverse outcomes or desired biological effects to exploit NP-protein conjugates for biomedical applications while circumventing possible deficits in their safety profile. The prevailing approaches for monitoring changes in the secondary and tertiary structure of proteins include methods like circular dichroism, infrared spectroscopy and nuclear magnetic resonance spectroscopy [41,42]. However, these methods do not directly link the detected structural alterations with a certain biological response or functionality, whereas the huRBL mediator release assay enables direct assessment of an adverse outcome, *i.e.* allergic effects in sensitised patients which can be correlated with conformational changes resulting from binding to the NPs. Hence, using the huRBL assay to directly link conformational changes or specific orientations of an allergen with an altered allergic response provides a highly specific and clinically relevant *in vitro* method to investigate the allergenic activity [43,44].

In silico protein corona modelling – adsorption energies and preferred orientations

In silico modelling approaches were conducted first with UnitedAtom to model the adsorption energies and preferred orientations of the proteins of interest on the four differently coated SiO_2 NPs. The calculated minimum adsorption energies of the eight proteins used for modelling were ranked (Table 5) to display the predicted composition of the protein corona of the respective NP types. For the modelling approach, ζ- potential values of the NPs determined in H_2O and pH 4 buffer were used (Table 2). The calculated adsorption energies for all possible orientations with the corresponding angles ϕ and θ were plotted in heatmaps to identify the preferred orientations of each protein on the respective NP surface (Supplementary Figs. S1-S8). As listed in Table 5, ovalbumin gave the highest binding affinity to all four types of NPs, which indicates that it would be the most abundant protein in the respective protein corona if this was determined by binding affinity alone (just based on NP-protein interactions irrespective of the resulting lateral protein-protein interactions even in case of a monolayer). The highest binding affinity was predicted for APTES-coated SiO_2 NPs in water, and for PTMO-coated SiO_2 NPs in pH 4 buffer. Ovalbumin was followed by serotransferrin and Bet v 6 in the ranking of the adsorption energies. These three proteins possess the largest molecular weights of the eight applied proteins (MW in Table 1), ranging from 34.2 kDa to 75.2 kDa, whereas all other proteins are in a MW range between 9 and 18 kDa. It may be suspected that the *in silico* modelling tool predicted stronger binding affinities for the proteins with larger molecular weights, as they possess a higher number of amino acids that interact with the NP. The calculated adsorption energies (Table 5) for one NP were largely independent of variations in the ζ-potential value for all proteins. This indicates that variation of NP physicochemical properties, such as surface charge, does not have a very strong influence on the predictions of the modelling tool. Overall, the adsorption energies of each protein were within a very narrow range for all four NPs, indicating that approximating the surface modifications with different functional groups by varying the surface potential did not have much impact on the predictions. This is not unexpected, since varying the surface potential only impacts charged residues, while realistically surface modifications may be expected to alter the hydrophobicity and binding properties of all amino acids. These results were subsequently compared with the experimental results obtained by binding selectivity studies using an artificial protein mix and birch pollen extract, to assess the reliability of our *in silico* modelling. However, comparing the entries of Table 5 (modelling results) with those in Table 4 (experimental results) clearly showed a lack of correlation between the predicted adsorption energies and the experimentally determined composition of the protein corona.

Fig. 6 depicts the most likely orientation(s) of Bet v 1 on the four differently coated SiO_2 NPs predicted by UnitedAtom. The heatmaps A-D in Fig. 6 display the predicted adsorption energies for all possible orientations of Bet v 1 on the respective NP surface. The dark blue areas coincide with the adsorption energies and corresponding angles ϕ and θ shown in Fig. 6E. The strongest binding of Bet v 1 to the NPs in H_2O, was predicted for APTES-coated SiO_2 NPs, followed by TSUA-coated, PTMO-coated and bare SiO_2 NPs. In contrast, the strongest binding was predicted for PTMO-coated NPs, followed by bare, APTES-coated and TSUA-coated NPs, using ζ-potential values determined in pH 4 buffer. These results contradict the experimentally observed binding behaviour of Bet v 1 with the four differently coated SiO_2 NPs (Fig. 3). According to these experimental results, the TSUA-coated NPs showed the highest binding capacity for Bet v 1 in all three examined buffers with varying pH values, and the APTES-coated NPs revealed the lowest binding capacity.

Furthermore, the heatmaps (Fig. 6A-D) appeared to be very similar, which indicated that the binding orientation of Bet v 1 would be similar for all four NPs, independent of the surface modifications. In contrast, the experimental results of the huRBL mediator release assay indicated a difference in orientation or structural alterations when Bet v 1 was bound to the TSUA-coated NPs. This may further imply a potential alteration in epitope accessibility of Bet v 1 mediated by the hydrophobic and negatively charged particle functionalisation. Notably, a partial unfolding of Bet v 1 due to interference of the undecanoic acid chain with the hydrophobic inner core of the protein cannot be ruled out.

To further investigate the correlation between *in vitro* and *in silico* results, we performed a numerical simulation of the corona formation with the CoronaKMC tool for the set of proteins beta-lactoglobulin, serotransferrin, ovalbumin and lysozyme on the unmodified SiO_2 NP of radius $R = 40$ nm, taking the ζ-potential to be 0 mV. The time-dependent corona dynamics are shown in Fig. 7, where we have summed over all orientations for each protein to

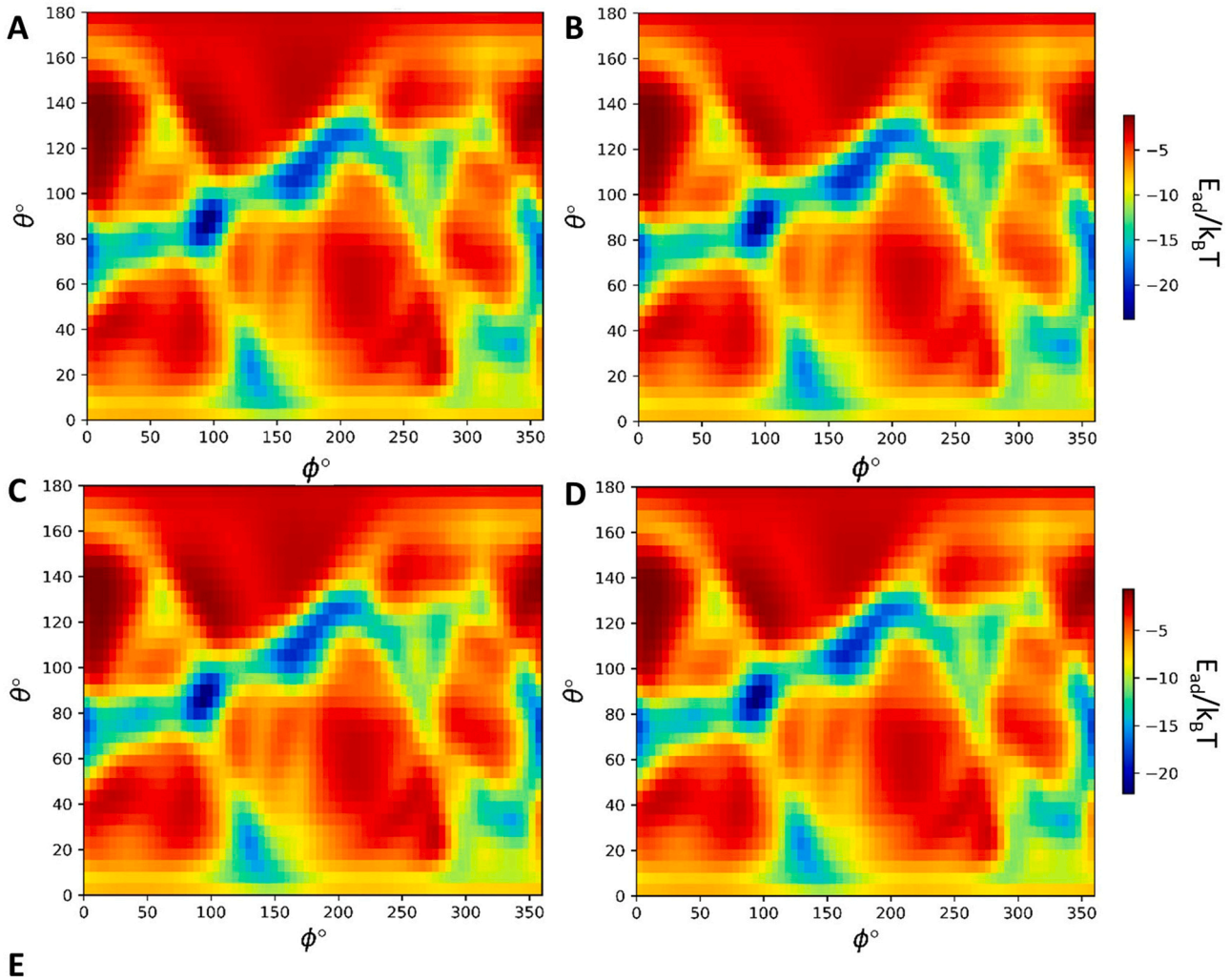

E

SiO_2 NP Type	E_{ad}/k_BT ζ H_2O / pH 4	Angle ϕ ζ H_2O / pH 4	Angle θ ζ H_2O / pH 4
Bare	-29.05 / -30.21	90 / 90	80 / 80
APTES	-31.81 / -30.2	90 / 95	80 / 85
TSUA	-29.51 / -29.35	90 / 95	80 / 85
PTMO	-29.48 / -31.01	90 / 90	80 / 80

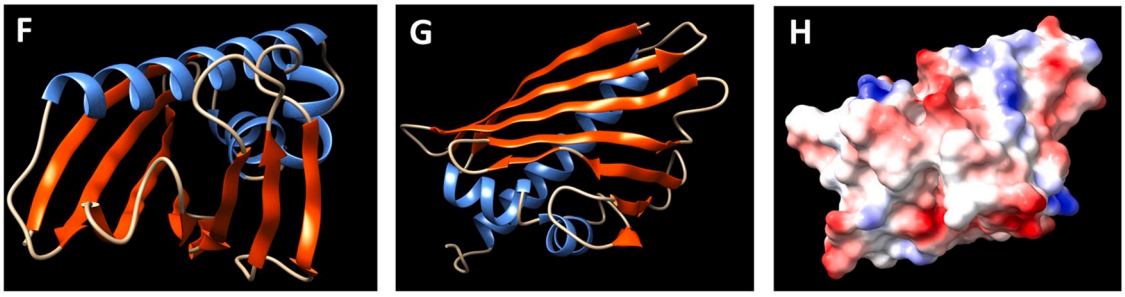

(caption on next page)

Fig. 6. Orientation-specific binding energy of Bet v 1 (PDB-ID 4A88) on SiO_2 NPs determined in silico with UnitedAtom. (A) Bare (B) APTES- (C) TSUA- (D) PTMO-coated SiO_2 NPs. ζ-potentials of particles used for modelling were determined in H_2O. (E) Minimum adsorption energy and corresponding angles of Bet v 1 interacting with differently coated silica NPs. ζ-potentials of particles used for modelling were determined in H_2O and pH 4 buffer. Angles ϕ and θ correspond to specific orientations of the protein on the NP surface, determined by rotation around the Y and Z axes of the corresponding PDB 3D structure of the protein. All minimum adsorption energy values are reported in units of k_BT (Boltzmann constant at Temperature in Kelvin) T = 300 K. 1 k_BT = 2.494 kJ/mol. Ribbon representation of 3D protein model with PDB-ID 4A88 as retrieved from PDB (F) and upon rotation by angles Φ and Θ (G) and surface charge representation (pos. charge in blue, neg. in red) of rotated 3D protein model (H). All 3D protein representations were produced from respective PDB files using UCSF Chimera (https://www.rbvi.ucsf.edu/chimera/), developed by the Resource for Biocomputing, Visualization, and Informatics at the University of California, San Francisco, with support from NIH P41-GM103311 (DOI: 10.1002/jcc.20084).

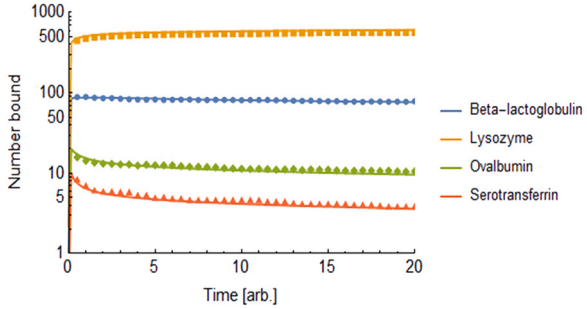

Fig. 7. Predicted number abundances of each protein in the hard corona of a bare silica NP of radius 40 nm as a function of time, obtained from numerical solutions to the set of coupled rate equations in the hard-sphere model (lines) and a kinetic Monte Carlo simulation (points, single trajectory showing the average over 10 NPs simulated simultaneously).

Table 6
Details of the in silico hard corona abundances (number of proteins of each type per NP) predicted from the rate equation approach (CoronaKMC, evaluated at t = 1000 arb. units, see Fig. 7) compared to the numbers extracted from corona binding experiments (Table 4). Sero (Serotransferrin), Ova (Ovalbumin), BLG (Beta-lactoglobulin a), Lyso (Lysozyme).

				Number per NP	
Protein	conc. bound	mass	conc. bound		Rate equation
	[mg/L]	(g/mol)	[microM]	Experimental	(steady-state)
BLG	51	18,400	2.77174	1965.3	47.0
Sero	10.3	75,690	0.136081	96.5	1.7
Ova	44.1	42,700	1.03279	732.3	4.6
Lyso	28.4	14,400	1.97222	1398.4	710

show the total number of each type of protein as a function of time. We plotted both the rate-equation approach in which different protein orientations are averaged together and the KMC approach in which all protein orientations are recorded separately, finding excellent agreement. We extracted the long-term limit of the number of bound proteins of each type from the rate equation model at $t = 1000$ arbitrary units, at which point the steady-state has been reached. The equivalent experimental quantity was obtained from the abundance fraction, the known initial weight concentration of 100 mg/L and the protein molecular weights, and the values obtained are summarised in Table 6. The ranking of these relative to the experimental ranking was significantly improved compared to the ranking by binding energy alone (predicted *via* UnitedAtom), with the two most strongly binding proteins switched but the others being correctly predicted. That is, the computational method predicts the ordering Lyso > BLG > Ova > Sero compared to the experimental ordering BLG > Lyso > Ova > Sero. We note that the same experimental ordering (Table 4) was achieved for both the bare silica NPs and the APTES-coated NPs, suggesting that the NP-protein interaction does not uniquely determine the corona composition. Thus, these results highlight the requirement to consider factors beyond the binding energy (namely, binding kinetics to account for differences in abundances and affinities) in predicting the corona composition. The absolute number of proteins bound in the computational corona, however, is significantly lower than the experiments indicate in which the amount of protein bound is far higher than even an optimal packing of proteins around the surface of the NP can achieve. This suggests the formation of multiple layers of the corona in the experimental case, which is not accounted for in the present model of corona formation and is likely dominated by protein-protein interactions rather than those between proteins and NPs, as supported by the observation that the ranking does not depend strongly on the NP surface.

Alignment of predicted corona with experimental data – limitations and potentials

Evaluation of the alignment of *in silico* protein corona modelling with *in vitro* investigations on protein corona formation and identification of areas of divergence and their causes may provide important pointers as to how to further improve the prediction capacities of emerging corona modelling tools and contribute to a better understanding of the resulting biological outcomes of corona formation. Therefore, assessment and identification of the potentials and limitations of current modelling procedures are imperative at this stage.

The initially applied modelling tool UnitedAtom (accessible *via* the NC KB) directly relates specific physicochemical characteristics of NPs with protein adsorption affinities. The synthesised SiO_2 NPs were modified with different functional groups to alter their physicochemical properties such as surface charge and hydrophobicity. Furthermore, the *in silico* tool allows ranking of several proteins by their adsorption affinities, which enables a first prediction of the protein corona composition. In the experimental workflow, artificial protein mixtures and birch pollen extract (BPE), a natural highly complex mixture, were incubated with differently coated SiO_2 NPs and protein binding was monitored quantitatively to reveal potential selectivity and ultimately compare *in silico* and *in vitro* results. Finally, the *in silico* tool predicted the most likely orientation of a protein on a NP surface *via* stepwise rotation of the protein's 3D structure relative to the NP surface and determination of corresponding adsorption energies for each orientation with the corresponding angles ϕ and θ. This allows the prediction of a specifically preferred orientation *vs.* randomised orientation of the protein of interest on the NP surface. A specific orientation could induce alterations in the biological outcome, in particular in respect to immune responses due to epitope hiding or accumulation. To address this experimentally, an allergenic effector cell degranulation assay (huRBL assay) was conducted to investigate the orientation and possible conformational changes of Bet v 1-NP conjugates, resulting in altered biological effects, *i.e.* alterations in the allergic response due to altered epitope accessibility.

Comparison of the experimentally obtained results with the calculated adsorption affinities and predicted orientations derived from the *in silico* modelling procedure with UnitedAtom revealed, however, substantial deviations. The ranking of proteins by adsorption energy (obtained by UnitedAtom) did not coincide with the actual corona composition determined by experimental binding studies, as can be expected from the neglect of the effects due to the size and concentration of each protein available for binding in the initial exposure solution. A better agreement was found when employing a hard-sphere corona model (CoronaKMC) taking into account the number concentrations and size of each protein. This

model predicts the content of the hard corona directly adsorbed to the surface of the NP, whereas the experimental approach reports the total corona which additionally includes the weakly-bound soft layers of proteins adsorbed to other proteins. Thus, a perfect agreement is not expected, especially given that the experimental results indicate the formation of multiple layers of soft corona. An extension of the model to account for these layers requires careful specification of the protein-protein interaction potentials and is presently under development.

Moreover, the modelling results with UnitedAtom suggested a similar binding orientation of Bet v 1 on all four types of NPs. This contradicted the experimental results of the huRBL assay, where a decreased allergenic response, due to alterations of the 3D structure or orientation of Bet v 1 leading to decreased IgE epitope accessibility, could be observed only for one type (TSUA-coated) of Bet v 1-SiO_2 NP conjugates.

One reason for these observed deviations might be an insufficient accounting for the environmental conditions that influence the protein-NP interaction in the UnitedAtom model. Since our experimental results, in accordance with previous studies [45,46], showed that environmental factors, like pH value, molarity and temperature determine the mode and quality of interaction between NPs and proteins to a great extent, adequately reflecting different environmental conditions in the model might be very important for the predictive power of modelling tools. The *in silico* modelling tools developed thus far could address the impact of different environmental conditions only by simulating varying surface potentials of the NPs. However, the altered electrostatic surface potentials of the proteins, depending on the pH of the surrounding medium, were not taken into account. In principle, the variation of the protein charge as a function of pH can be partially accounted for by updating the residues defined in the PDB input file according to their charge state as estimated using the PROPKA package [47,48] and using the potentials generated for these alternate residues rather than those for the amino acids under standard conditions. We found, however, that this produced only a minor variation in the predicted binding energies (Supplementary Fig. S9). A much more substantial difference, similar to that observed experimentally, is likely due to changes in the protein structure which cannot be accounted for by this method. As of yet, *in silico* protein structure prediction methods do not enable the prediction of the structure at arbitrary pH, and so at present the methodology is limited to neutral pH unless experimental structures are available at the target pH. Moreover, the potentials of mean force were calculated for individual amino acids, while interactive and compensating charges of neighbouring amino acids in the folded tertiary structure of proteins could not be simulated. This might, in general, be a substantial limitation of coarse-grained united atom protein corona modelling approaches [49]. At present, however, fully atomistic simulations of the binding of a single protein are extremely computationally demanding, and performing a simulation of many proteins binding over an extended period of time such as is required to simulate corona formation is not feasible.

Furthermore, the surface functionalisation of NPs is an important determinant of the protein-NP interaction, since the proteins may interact much less with the core of the NP, but rather with the functional groups exposed on the NP surface. While our experimental binding studies showed clear differences in the proteins´ binding behaviour depending on the differences in surface charge and hydrophobicity of the differently coated NPs, the modelling results were almost identical for all NPs irrespective of coating type. For the modelling approach, pre-calculated values of potentials of mean force and Hamaker constants for an SiO_2 surface with all 20 proteinogenic amino acids were used. The different surface functionalisation of the NPs was considered only *via* variation of the ζ-potential values. Therefore, it might be advisable to calculate new values for potentials of mean force and Hamaker constants directly for the actual functional groups exposed on the NP surface and interacting with the proteins. Thus, integrating further settings for different types of surface functionalisation could further improve the prediction certainties of modelling approaches.

Another relevant feature may be to incorporate the contribution of hydrophobic interactions into the calculation of adsorption affinities, besides electrostatic and van der Waals interactions. Our experimental results indicated, in accordance with previous findings [8], that hydrophobic interactions play a crucial role during corona formation, as the TSUA-coated NPs, possessing a highly hydrophobic character due to the long carbon chain of the coating, showed the highest binding capacity in addition to altered epitope accessibility. Excluding hydrophobic interactions *per se*, may thus limit the predictive power of modelling tools. Currently, the hydrophobic effects are only included in the UnitedAtom tool for amino acid-NP interactions, but not for the coating. If modelling tools could additionally incorporate hydrophobic interactions, *e.g., via* the development of novel NP descriptors similar to recently developed protein descriptors like the GRAVY (grand average of hydropathy) [50], it might become possible to predict potential disruptions in the tertiary structure of the adsorbed protein, potentially due to hydrophobic interactions, and thus in the resulting biological outcome. In particular, in light of the observations presented here, this might be desired and would facilitate better predictability of adverse biological outcomes of protein-NP conjugates and further improve risk assessment of NP biocompatibility.

As optimisation potential for the data output of the UnitedAtom modelling tool, a direct structural connection between the results from the modelling tool with orientations found in the PDB was identified, as this would aid its applicability by the user. In particular, for experimentalists, it might be very important to directly assign the calculated adsorption energies and the corresponding rotation angles to the respective PDB structure of the protein to enable a view on *e.g.*, immunological epitopes of the respective biomolecules. For example, in this study the ability to predict whether IgE epitopes are hidden or even accumulate at the NP surface would allow to directly determine whether a reduced or potentially increased allergenic response depends on orientation or conformational integrity of the bound allergen. Consequently, a script for extracting the optimum binding configuration from UnitedAtom output and an input PDB file has been developed and added to the NanoCommons Knowledge Base-accessible protein corona prediction tool generating a PBD output file providing the view from the particle surface onto the respective surface-bound area in the 3D model protein (Fig. 6 G+H).

A final direction that is worth considering in how to further improve the predictive capacity of models is to integrate predictions from physics-based models such as presented here, with predictions from data-driven models such as quantitative structure-activity relationship (QSAR) models or multi-variate models to correlate corona composition with cellular attachment [51]. For example, corona prediction models have been developed based on k Nearest Neighbours (kNN) approaches utilising datasets of coronas on gold nanoparticles of different sizes and surface fuctionalisations, based on the actual proteins bound to the library of NPs [52] (although it is notable that the method of isolation of the corona proteins in the original study (trichloroacetic acid in acetone) inadvertently removed albumin from the coronas of all particles, where albumin would be present *in situ* in the corona) [53]. Integrating both physics-based and data-driven predictive modelling of NPs corona composition and effects, for example into Intregrated Approaches to Testing and Assessment may enable the issues identified here in terms of limitations to the physics-based models to be overcome.

Conclusions

Alignment of data derived from *in vitro* experimentation with data from *in silico* modelling procedures is important in order to further optimise prediction capability of tools for protein corona formation and to improve computational approaches resulting in higher certainties. This could ultimately aid nano-related risk assessment, accelerate the design of NPs for medical applications, nano-agriculture, environmental sensing, to name just a few, and, in general, will help to consolidate investigations at the bio-nano interface and thus fill data gaps, including for corona formation with lipids, metabolites, or other (bio)molecules.

In this study, the intentional alignment of an experimental analysis with *in silico* protein corona predictions, at first, revealed substantial deviations between results, while the troubleshooting resulted in significant improvements in the alignment of the predictions with the experimental data. Employing an iterative optimisation process through mutual exchange between experimentalists and modellers, we identified the potentials and limitations of the current protein corona modelling tool UnitedAtom and listed recommendations that were ultimately applied and to a certain level integrated into the current CoronaKMC model to obtain a satisfying correlation between experiment and prediction. In summary, these recommendations comprised of (i) including environmental parameters, like pH value, influencing the protein binding to a great extent, into the simulations, (ii) consideration of compensating charges of neighbouring amino acids of folded proteins, (iii) inclusion of functional groups of NP coatings into the calculations of potentials of mean force and Hamaker constants, to reflect also the effects of hydrophobic interactions besides electrostatic and van der Waals forces, and (iv) enabling of a direct assignment of predicted adsorption regions to the proteins 3D structure to facilitate the identification of possible regions of accessible epitopes for biologic reactions by experimentalists.

To promote data FAIRness, we compiled the entire experimental dataset including the corresponding metadata and uploaded it to a data repository for easy access and long-term storage, and to the NC KB, to facilitate interactive re-use of data directly *via* the corona prediction model or for integration into other modelling tools and datasets.

In summary, *in silico* protein corona modelling tools have great potential to support and accelerate experimental investigations including the process of protein corona formation. Nevertheless, several refinements still need to be made to simulate the actual conditions of protein-NP interactions in a more accurate way. A clear understanding of the molecular events occurring during bio-nano interactions, with a special focus on protein structure and function, may result in a more reliable prediction of potential adverse biological outcomes or ultimately even enable the design/engineering of protein-NP conjugates for optimal safety and function. Overall, protein corona modelling tools may thus support, improve and accelerate biocompatibility assessment of NPs. Co-development and systematic improvement of the *in silico* models' predictive capacities, as presented for the protein corona tools here, will enable greater trust in computational predictions, aid data enrichment, and accelerate hazard assessment in future.

Data Availability

All data generated during this study are included in this published article and the supplementary information. Physicochemical characterisation data including relevant metadata for the differently coated SiO_2 NPs, as well as *in vitro* investigations and *in silico* predictions of protein corona formation with UnitedAtom have been deposited in the NanoCommons Knowledge Base (https://ssl.biomax.de/nanocommons/) and are additionally accessible at Zenodo (https://doi.org/10.5281/zenodo.4609839). Source code of the UnitedAtom tool is available at https://bitbucket.org/softmattergroup/unitedatom/src/master/.

Declaration of Competing Interest

The authors declare that they have no known competing financial interests or personal relationships that could have appeared to influence the work reported in this paper.

Acknowledgments

This work was funded by the European Commission Horizon 2020 (H2020) research infrastructure for nanosafety project NanoCommons (grant agreement 731032), the H2020 Research and Innovation grant NanoSolveIT (grant agreement 814572), the International Doctoral School "Immunity in Cancer and Allergy - ICA" of the Austrian Science Fund, Austria (FWF, grant W01213), and the Allergy-Cancer-BioNano Research Center of the PLUS. We would like to acknowledge Milena Schenck for providing the PTMO-coated SiO_2 NPs. The authors acknowledge the Transnational Access provision from NanoCommons to Robert Mills-Goodlet.

Author contributions

IH performed the experimental work for Figs. 1–5 and Tables 2–4 and wrote the first draft of the manuscript. RMG performed the *in silico* modelling with UnitedAtom for Fig. 6, Figs. S1-S8 and Table 5. LJ contributed to the experimental work for Fig. 5. MG operated the TEM, DLS and ELS equipment. IR and VL provided and helped with use of the *in silico* tool UnitedAtom and performed predictions of corona abundances and kinetic MC calculations. DM provided access and support for working with the NanoCommons Knowledge Base. AD and IL provided funding and infrastructure for performing this study. MH supervised and conceived the study and provided infrastructure and funding for the study. All authors critically reviewed and edited the manuscript.

Ethics approval and consent to participate

The collection and usage of patient samples for the huRBL assay was approved by the local Ethics Committee of the Allergy Clinic Salzburg (No. 415-E/1398/4–2011).

Appendix A. Supporting information

Supplementary data associated with this article can be found in the online version at doi:10.1016/j.nantod.2022.101561.

References

[1] S. Kumar, et al., Structure and interaction of nanoparticle–protein complexes, Langmuir 34 (20) (2018) 5679–5695.
[2] X. Tian, Y. Chong, C. Ge, Understanding the nano–bio interactions and the corresponding biological responses, Frontiers in Chemistry, 8 (2020) 446.
[3] E. Mostafavi, P. Soltantabar, T.J. Webster, Nanotechnology and picotechnology: a new arena for translational medicine, Biomaterials in Translational Medicine 9 Elsevier, 2019, pp. 191–212.
[4] A. Solanki, J.D. Kim, K.-B. Lee, Nanotechnology for regenerative medicine: nanomaterials for stem cell imaging, Nanomedicine 3 (4) (2008) 592–613.
[5] S.P. Forster, S. Olveira, S. Seeger, Nanotechnology in the market: promises and realities, Int. J. Nanotechnol. 8 (6–7) (2011) 592–613.
[6] J. Lee, S. Mahendra, P.J. Alvarez, Nanomaterials in the construction industry: a review of their applications and environmental health and safety considerations, ACS Nano 4 (7) (2010) 3580–3590.
[7] F. Barbero, et al., Formation of the protein corona: the interface between nanoparticles and the immune system. in, Seminars in Immunology 34 Elsevier, 2017, pp. 52–60.

[8] T. Cedervall, et al., Understanding the nanoparticle–protein corona using methods to quantify exchange rates and affinities of proteins for nanoparticles, Proc. Natl. Acad. Sci. 104 (7) (2007) 2050–2055.
[9] I. Lynch, et al., The nanoparticle–protein complex as a biological entity; a complex fluids and surface science challenge for the 21st century, Adv. Colloid Interface Sci. 134 (2007) 167–174.
[10] D.A. Winkler, et al., Modelling and predicting the biological effects of nanomaterials, SAR QSAR Environ. Res. 25 (2) (2014) 161–172.
[11] C.O. Hendren, et al., The nanomaterial data curation initiative: a collaborative approach to assessing, evaluating, and advancing the state of the field, Beilstein J. Nanotechnol. 6 (1) (2015) 1752–1762.
[12] A. Afantitis, et al., NanoSolveIT Project: driving nanoinformatics research to develop innovative and integrated tools for in silico nanosafety assessment, Comput. Struct. Biotechnol. J. 18 (2020) 583–602.
[13] C.M. Powers, et al., Nanocuration workflows: establishing best practices for identifying, inputting, and sharing data to inform decisions on nanomaterials, Beilstein J. Nanotechnol. 6 (1) (2015) 1860–1871.
[14] R.L.M. Robinson, et al., How should the completeness and quality of curated nanomaterial data be evaluated? Nanoscale 8 (19) (2016) 9919–9943.
[15] A. Ammar, et al., A semi-automated workflow for FAIR maturity indicators in the life sciences, Nanomaterials 10 (10) (2020) 2068.
[16] A.G. Papadiamantis, et al., Metadata stewardship in nanosafety research: community-driven organisation of metadata schemas to support FAIR nanoscience data, Nanomaterials 10 (10) (2020) 2033.
[17] M.D. Wilkinson, et al., The FAIR guiding principles for scientific data management and stewardship, Sci. data 3 (1) (2016) 1–9.
[18] Z.J. Deng, et al., Plasma protein binding of positively and negatively charged polymer-coated gold nanoparticles elicits different biological responses, Nanotoxicology 7 (3) (2012) 314–322.
[19] M. Kopp, S. Kollenda, M. Epple, Nanoparticle–protein interactions: therapeutic approaches and supramolecular chemistry, Acc. Chem. Res. 50 (6) (2017) 1383–1390.
[20] F. Turci, et al., An integrated approach to the study of the interaction between proteins and nanoparticles, Langmuir 26 (11) (2010) 8336–8346.
[21] S.R. Saptarshi, A. Duschl, A.L. Lopata, Interaction of nanoparticles with proteins: relation to bio-reactivity of the nanoparticle, J. Nanobiotechnol. 11 (1) (2013) 26.
[22] D. Power, et al., A multiscale model of protein adsorption on a nanoparticle surface, Model. Simul. Mater. Sci. Eng. 27 (8) (2019) 084003.
[23] I. Rouse, V. Lobaskin, A hard-sphere model of protein corona formation on spherical and cylindrical nanoparticles, Biophys. J. 120 (2021) 4457–4471.
[24] W. Stöber, A. Fink, E. Bohn, Controlled growth of monodisperse silica spheres in the micron size range, J. Colloid Interface Sci. 26 (1) (1968) 62–69.
[25] M. Avella, et al., Poly (ε-caprolactone)-based nanocomposites: Influence of compatibilization on properties of poly (ε-caprolactone)–silica nanocomposites, Compos. Sci. Technol. 66 (7–8) (2006) 886–894.
[26] A. Feinle, et al., Stable carboxylic acid derivatized alkoxy silanes, Chem. Commun. 51 (12) (2015) 2339–2341.
[27] C.A. Schneider, W.S. Rasband, K.W. Eliceiri, NIH Image to ImageJ: 25 years of image analysis, Nat. Methods 9 (7) (2012) 671–675.
[28] D.D. Varsou, et al., Zeta-potential read-across model utilizing nanodescriptors extracted via the nanoxtract image analysis tool available on the enalos nanoinformatics cloud platform, Small 16 (21) (2020) 1906588.
[29] B. Grotz, et al., Biologic effects of nanoparticle-allergen conjugates: time-resolved uptake using an in vitro lung epithelial co-culture model of A549 and THP-1 cells, Environ. Sci. Nano 5 (9) (2018) 2184–2197.
[30] L. Vogel, et al., Development of a functional in vitro assay as a novel tool for the standardization of allergen extracts in the human system, Allergy 60 (8) (2005) 1021–1028.
[31] M. Mahmoudi, et al., Cell toxicity of superparamagnetic iron oxide nanoparticles, J. Colloid Interface Sci. 336 (2) (2009) 510–518.
[32] F. Darabi Sahneh, C. Scoglio, J. Riviere, Dynamics of nanoparticle-protein corona complex formation: analytical results from population balance equations, PloS One 8 (5) (2013) e64690.
[33] D. Dell'Orco, et al., Modeling the time evolution of the nanoparticle-protein corona in a body fluid, PloS One 5 (6) (2010) e10949.
[34] Wolfram Research, Inc., Mathematica, Version 12.1, 2020, Champaign, Illinois, USA.
[35] J.M. Berg, et al., The relationship between pH and zeta potential of~ 30 nm metal oxide nanoparticle suspensions relevant to in vitro toxicological evaluations. Nanotoxicology 3 (4) (2009) 276–283.
[36] J. Coates, Interpretation of infrared spectra, a practical approach, in: R.A. Meyers (Ed.), Encyclopedia of Analytical Chemistry: Applications, Theory and Instrumentation, 2006, pp. 10815–10837.
[37] A.B.D. Nandiyanto, R. Oktiani, R. Ragadhita, How to read and interpret FTIR spectroscope of organic material, Indones. J. Sci. Technol. 4 (1) (2019) 97–118.
[38] J. Lahiri, et al., A strategy for the generation of surfaces presenting ligands for studies of binding based on an active ester as a common reactive intermediate: a surface plasmon resonance study, Anal. Chem. 71 (4) (1999) 777–790.
[39] E. Gasteiger, et al., Protein identification and analysis tools on the ExPASy server. The proteomics protocols handbook, 2005: p. 571–607.
[40] R. Mills-Goodlet, et al., Biological effects of allergen-nanoparticle conjugates: uptake and immune effects determined on hAELVi cells under submerged vs. air-liquid interface conditions, Environ. Sci.: Nano 7 (2020) 2073–2086.
[41] L. Calzolai, et al., Protein– nanoparticle interaction: identification of the ubiquitin– gold nanoparticle interaction site, Nano Lett. 10 (8) (2010) 3101–3105.
[42] J.J. Gray, The interaction of proteins with solid surfaces, Curr. Opin. Struct. Biol. 14 (1) (2004) 110–115.
[43] H. Hoffmann, et al., The clinical utility of basophil activation testing in diagnosis and monitoring of allergic disease, Allergy 70 (11) (2015) 1393–1405.
[44] N. Sun, et al., Use of a rat basophil leukemia (RBL) cell-based immunological assay for allergen identification, clinical diagnosis of allergy, and identification of anti-allergy agents for use in immunotherapy, J. Immunotoxicol. 12 (2) (2015) 199–205.
[45] T. Kopac, K. Bozgeyik, J. Yener, Effect of pH and temperature on the adsorption of bovine serum albumin onto titanium dioxide, Colloids Surf. A Physicochem. Eng. Asp. 322 (1–3) (2008) 19–28.
[46] M. Mahmoudi, et al., Protein– nanoparticle interactions: opportunities and challenges, Chem. Rev. 111 (9) (2011) 5610–5637.
[47] M.H. Olsson, et al., PROPKA3: consistent treatment of internal and surface residues in empirical p K a predictions, J. Chem. Theory Comput. 7 (2) (2011) 525–537.
[48] C.R. Søndergaard, et al., Improved treatment of ligands and coupling effects in empirical calculation and rationalization of p K a values, J. Chem. Theory Comput. 7 (7) (2011) 2284–2295.
[49] T. Casalini, et al., Molecular modeling for nanomaterial–biology interactions: Opportunities, challenges, and perspectives, Front. Bioeng. Biotechnol. 7 (2019) 268.
[50] Y. Duan, et al., Prediction of protein corona on nanomaterials by machine learning using novel descriptors, NanoImpact 17 (2020) 100207.
[51] C.D. Walkey, et al., Protein corona fingerprinting predicts the cellular interaction of gold and silver nanoparticles, ACS Nano 8 (3) (2014) 2439–2455.
[52] A. Afantitis, et al., A nanoinformatics decision support tool for the virtual screening of gold nanoparticle cellular association using protein corona fingerprints, Nanotoxicology 12 (10) (2018) 1148–1165.
[53] A.J. Chetwynd, K.E. Wheeler, I. Lynch, Best practice in reporting corona studies: minimum information about Nanomaterial Biocorona Experiments (MINBE), Nano Today 28 (2019) 100758.